American Mineralogist, Volume 73, pages 1370–1376, 1988

Thermal behavior of the crystal structure of strontian piemontite

MICHELE CATTI
Dipartimento di Chimica Fisica ed Elettrochimica dell 'Università, via Golgi 19, 20123 Milano, Italy
GIOVANNI FERRARIS, GABRIELLA IVALDI
Dipartimento di Scienze della Terra dell 'Università, Sezione di Mineralogia e Cristallografia, via S. Massimo 24, 10123 Torino, Italy

ABSTRACT

Unit-cell constants of a strontian-piemontite sample from St. Marcel (Val d'Aosta, Italy) with composition $Ca_{1.80}Sr_{0.20}Al_{1.91}Fe_{0.33}Mn_{0.82}Si_3O_{12}OH$ were measured at several temperatures by single-crystal X-ray diffractometry (Mo$K\alpha$ radiation). Values at 25 and 800 °C are $a = 8.884(3)$, $b = 5.684(1)$, $c = 10.202(3)$ Å, $\beta = 115.23(2)°$; and $a = 8.934(9)$, $b = 5.727(4)$, $c = 10.30(1)$ Å, $\beta = 115.26(9)°$, respectively, for space group $P2_1/m$. Principal coefficients of thermal expansion are 0.72×10^{-5}, 0.98×10^{-5}, and 1.29×10^{-5} K^{-1}. Intensity data were measured at 25 and 800 °C, respectively, and the corresponding least-squares refinements of the crystal structure converged to $R = 0.041$ and 0.056. The thermal-expansion ellipsoid is symmetrically oriented with respect to **a** and **c**. A significant shrinking of the Si_2O_7 group, with opening of the Si–O–Si angle, is observed at high temperature. A large and very anisotropic mean expansion (1.4×10^{-5} K^{-1}) occurs for the (Mn,Fe) coordination octahedron [M(3) site]. The relation between thermal expansion of the lattice and thermal expansion of the coordination polyhedra is accounted for by a correlated tilting of polyhedra at high temperature. No deprotonation can be detected before the breakdown of the structure (880 °C); the dehydration products have been identified.

INTRODUCTION

In the framework of a research program on the high-temperature crystal chemistry of rock-forming minerals containing OH groups, results concerning magnesiochloritoid were previously published (Ivaldi et al., 1988) and a study of piemontite is presented here. This mineral, which belongs to the epidote-clinozoisite family, is common in low-grade metamorphic rocks derived from Mn-rich sediments and also occurs as a late-crystallizing phase in acid and intermediate volcanic rocks. The room-temperature crystal structure was refined by Dollase (1969); its main features, typical of the epidote family, are the presence of both isolated SiO_4 tetrahedra and Si_2O_7 ditetrahedra, and of chains of coordination octahedra of Al, Mn, and Fe sharing edges.

An aim of this high-temperature structural study is to investigate the thermal behavior of Si_2O_7 groups, as no other disilicate has been previously analyzed in this way. Another important result of this research is finding relations between the lattice thermal expansion, coordination-polyhedra expansion, and rotations or kinking of polyhedra linkages, in connection with the overall topology of the structure (Hazen and Finger, 1982). Finally, we are able to investigate at high temperature the structural role of OH groups and possible changes of cation distribution over different sites.

EXPERIMENTAL DETAILS AND STRUCTURE REFINEMENTS

A sample of piemontite crystals embedded in a calcite matrix from St. Marcel (Val d'Aosta, Italy) was used for all experiments; a survey of St. Marcel piemontites has been given by Mottana and Griffin (1982). Different crystals were analyzed by microprobe (standards were kaersutite, ardennite, and celestine), and the average of seven measurements yielded the following results: SiO_2, 35.03%; Al_2O_3, 19.27%; Fe_2O_3, 5.15%; Mn_2O_3, 12.74%; MgO, 0.085%; CaO, 19.81%; SrO, 4.09%; TiO_2 in traces (total 96.18%). On the basis of 12 oxygen atoms and one OH group, the atomic composition $Ca_{1.80}Sr_{0.20}Al_{1.91}Fe_{0.33}Mn_{0.82}Si_{2.96}O_{12}OH$ is obtained. The present sample shows one of the highest average Sr contents ever found in piemontite (Deer et al., 1986).

A single crystal with dimensions 0.5 × 0.1 × 0.1 mm was selected and mounted on a Nicolet R3 four-circle diffractometer, with graphite monochromator and Mo$K\alpha$ radiation, for all X-ray measurements. The crystal was affixed to a quartz-glass fiber with Ga-100 cement. The crystal was bathed in a stream of hot N_2, utilizing an A.E.T. thermal attachment with T monitored by a thermocouple, as described by Argoud and Capponi (1984). The lattice thermal expansion was studied by determining the unit-cell constants at 25, 300, 500, 600, 700, and 800 °C; in each case the temperature was stabilized for at least 3 h, and then the same 25 reflections with $48° < 2\theta < 60°$ were centered and their angular values refined, obtaining the results reported in Table 1. Diffraction intensities were measured at 25 and 800 °C.

0003–004X/88/1112–1370$02.00

Table 1. Lattice constants of piemontite at different temperatures (single crystal)

T (°C)	a (Å)	b (Å)	c (Å)	β (°)	V (Å^3)
25	8.884(3)	5.684(1)	10.202(3)	115.23(2)	466.0(2)
300	8.903(3)	5.697(1)	10.237(4)	115.24(3)	469.7(3)
500	8.919(4)	5.709(2)	10.263(5)	115.25(4)	472.6(4)
600	8.925(5)	5.714(2)	10.276(5)	115.26(5)	474.0(5)
700	8.930(6)	5.721(3)	10.290(7)	115.26(6)	475.5(6)
800	8.934(9)	5.727(4)	10.30(1)	115.26(9)	476.8(9)

Note: Estimated standard deviations are in parentheses.

Structure refinement at 25 °C

At room temperature [a = 8.884(3), b = 5.684(1), c = 10.202(3) Å, β = 115.23(2)°], 6636 reflections were collected from the hemisphere with $h \geq 0$ and by ω scan, with the following conditions: scan width = 2.5°, background time to scan time ratio = 0.5, scan speed ranging from 4.0 to 29.30 deg·min^{-1} with linear interpolation for intensities between 80 and 2500 counts s^{-1}. An empirical correction was applied for absorption (North et al., 1968), by measuring psi scans of seven high-chi reflections with different 2θ; the transmission coefficients ranged from 0.693 to 1. Intensities of equivalent reflections were averaged and those with $I \leq 2\sigma(I)$ were removed, leaving a set of 3385 independent observed data. The least-squares refinement of the crystal structure (space group $P2_1/m$, Z = 2) was started from the parameters published by Dollase (1969), using the RFINE program (Finger and Prince, 1975). The Ca/Sr and Al/(Mn,Fe) substitutions in the larger A and smaller M sites, respectively, were determined by refining the corresponding occupancies; the scattering factor of Mn was used for (Mn,Fe). No chemical constraint related to the microprobe analysis was introduced. With isotropic thermal factors, convergence [weights = $1/\sigma^2(F_o)$] was reached at R = 0.064, and the subsequent anisotropic refinement lowered R to 0.041. The overall chemical formula consistent with refined site occupancies is $Ca_{1.799}Sr_{0.201}Al_{1.869}(Mn,Fe)_{1.131}Si_3O_{12}OH$, which compares favorably with the average value obtained from microprobe analysis.

Structure refinement at 800 °C

At 800 °C [a = 8.934(9), b = 5.727(4), c = 10.30(1) Å, β = 115.26(9)°], 2826 diffraction intensities were measured ($2\theta \leq 70°$) with the following conditions: $\omega/2\theta$ scan, scan width variable between 2.2° and 2.7°, ratio of background time to scan time = 0.5, and scan speed ranging from 3.0 to 29.30 deg·min^{-1} with linear interpolation for intensities between 150 and 2500 counts s^{-1}. The limitation $-90° < \chi < 75°$ was required by the presence of the heating attachment and prevented the empirical absorption correction; inaccessible reflections were replaced by their equivalent ones by monoclinic symmetry. After averaging and removing reflections with $I \leq 2\sigma(I)$, 2180 unique observations were left for the least-squares refinement. Convergence [weights = $1/\sigma^2(F_o)$] was attained at R = 0.101 and 0.056 with isotropic and anisotropic thermal factors, respectively. At first, the electron contents of the A and M sites were left free to vary, giving a different composition from that at room temperature: $Ca_{1.833}Sr_{0.167}Al_{1.930}(Mn,Fe)_{1.070}Si_3O_{12}OH$. This drop in the amount of strongly scattering atoms (Mn, Fe, Sr) did not seem realistic because no evidence of segregation of different phases could be detected in the crystal. Consequently, the composition was fixed to the values obtained at 25 °C, and the refinement converged to the same R value as before. It can be concluded, therefore, that the apparent change of chemical contents was actually due to correlation between occupancy and thermal parameters combined with a higher thermal-motion increase with temperature for the A and M sites (Table 2). On the other hand, this thermal-motion increase should not be ascribed to a larger disorder, as the temperature factors of sites A(1) and M(2), which are occupied by a single atomic species, and of sites with atomic substitutions show comparable thermal increases. Such an effect probably is general and should warn against refining the chemical composition from data collected at high temperature.

Table 2. Atomic fractional coordinates and equivalent isotropic temperature factors (Å^2) of piemontite, at 25 °C (above) and 800 °C (below)

Site	Occupancy*	x	y	z	B_{eq}
A(1)	Ca: 1.000(2); Sr: 0.000	0.75896(6)	¾	0.15395(5)	0.87(1)
		0.7605(1)	¾	0.1550(1)	2.45(5)
A(2)	Ca: 0.799(3); Sr: 0.201	0.59844(5)	¾	0.42438(4)	0.92(1)
		0.5959(1)	¾	0.4208(1)	2.61(4)
M(1)	Al: 0.810(4); (Mn,Fe): 0.190	0	0	0	0.45(2)
		0	0	0	1.19(3)
M(2)	Al: 1.000(4); (Mn,Fe): 0.000	0	0	½	0.44(2)
		0	0	½	1.26(4)
M(3)	Al: 0.059(4); (Mn,Fe): 0.941	0.29468(4)	¼	0.22161(4)	0.48(1)
		0.29447(9)	¼	0.22185(9)	1.40(3)
Si(1)	1	0.34046(7)	¾	0.04491(7)	0.51(2)
		0.3390(1)	¾	0.0426(1)	1.21(5)
Si(2)	1	0.68461(7)	¼	0.27550(7)	0.51(2)
		0.6851(1)	¼	0.2757(1)	1.20(5)
Si(3)	1	0.18391(7)	¾	0.31827(7)	0.53(2)
		0.1841(1)	¾	0.3182(1)	1.16(5)
O(1)	1	0.2338(1)	0.9921(2)	0.0369(1)	0.84(3)
		0.2337(3)	0.9882(5)	0.0358(3)	2.2(1)
O(2)	1	0.3041(1)	0.9799(2)	0.3545(1)	0.76(3)
		0.3035(3)	0.9780(5)	0.3550(3)	2.0(1)
O(3)	1	0.7957(1)	0.0154(2)	0.3396(1)	0.68(3)
		0.7949(3)	0.0183(5)	0.3411(3)	1.7(1)
O(4)	1	0.0576(2)	¼	0.1312(2)	0.64(5)
		0.0598(4)	¼	0.1295(4)	1.5(1)
O(5)	1	0.0417(2)	¾	0.1465(2)	0.69(5)
		0.0433(4)	¾	0.1471(4)	1.6(1)
O(6)	1	0.0667(2)	¾	0.4068(2)	0.69(5)
		0.0656(4)	¾	0.4050(4)	1.8(1)
O(7)	1	0.5145(2)	¾	0.1792(2)	0.82(5)
		0.5117(4)	¾	0.1739(4)	2.1(1)
O(8)	1	0.5264(2)	¼	0.3124(2)	1.01(5)
		0.5250(4)	¼	0.3090(5)	2.7(2)
O(9)	1	0.6239(2)	¼	0.1000(2)	1.34(6)
		0.6301(6)	¼	0.1031(4)	3.6(2)
O(10)	1	0.0837(2)	¼	0.4308(2)	0.67(5)
		0.0811(4)	¼	0.4304(4)	1.7(1)
H*	1	0.055(5)	¼	0.350(5)	1.2(9)

Note: Estimated standard deviations are in parentheses.
* At 25 °C.

Final atomic fractional coordinates and occupancy factors with esd's, for both the 25 and the 800 °C refinements, are reported in Table 2.[1]

[1] A copy of structure factors and anisotropic thermal parameters may be ordered as Document AM-88-392 from the Business Office, Mineralogical Society of America, 1625 I Street, N.W., Suite 414, Washington, D.C. 20006, U.S.A. Please remit $5.00 in advance for the microfiche.

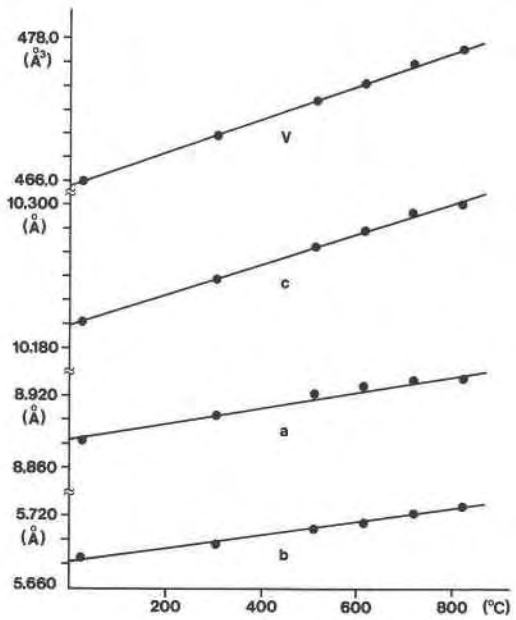

Fig. 1. Lattice parameters of piemontite at various temperatures; values and esd's in Table 1. Coefficients for regression lines are given in Table 3.

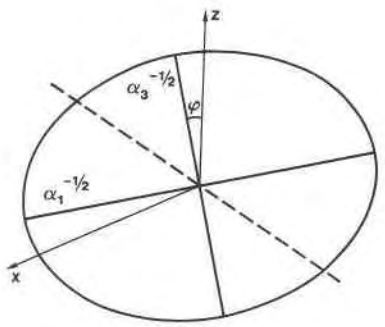

Fig. 2. (010) section of the ellipsoid of inverse square-root thermal expansion, calculated from linear-regression expansivities of Table 3 for piemontite.

Discussion

Thermal expansion

Unit-cell constants have been plotted against temperature in Figure 1, except for the angle β, which remains constant within the esd's (Table 1). A linear behavior is followed closely by *b*, *c*, and *V*, whereas the *a* edge shows a slight negative deviation from linearity at high temperature. Straight-line interpolations are drawn in Figure 1; the corresponding parameters and the resulting coefficients of thermal expansion have been reported in Table 3. By diagonalizing the tensor of thermal strain, the following values are obtained for principal coefficients of thermal expansion: $\alpha_1 = 0.72(4) \times 10^{-5}$, $\alpha_2 = 0.98(5) \times 10^{-5}$, and $\alpha_3 = 1.29(5) \times 10^{-5}$ K^{-1}; the principal axis α_2 is parallel to **b**, and the angle between the α_3 axis and **c** is $\Phi = 13°$. The (010) section of the ellipsoid with semi-axes equal to $\alpha_1^{-1/2}$, $\alpha_2^{-1/2}$, $\alpha_3^{-1/2}$, oriented properly with respect to the unit cell, is shown in Figure 2; the inverse of the squared radius of this ellipsoid along a particular crystallographic direction gives the corresponding thermal-expansion coefficient. It appears that the orientation of the ellipse of Figure 2 is symmetrical with respect to **a** and **c**, i.e., the bisectrixes of angles between **a** and **c** and between the ellipse semi-axes coincide; this orientation corresponds to the condition $\Phi = (\beta - 90°)/2$.

Such a result can be proven to necessarily hold when the monoclinic β angle is not changed by the lattice strain ($\beta' = \beta$). Then the components of the thermal-strain tensor (Schlenker et al., 1978) on the (010) plane become

$$\alpha_{11} = [(a' \sin \beta'/a \sin \beta) - 1]/\Delta T = [(a'/a) - 1]/\Delta T;$$
$$\alpha_{33} = [(c'/c) - 1]/\Delta T;$$
$$\alpha_{13} = [(a' \cos \beta'/a \sin \beta) - (c' \cos \beta/c \sin \beta)]/(2\Delta T)$$
$$= [(a'/a) - (c'/c)]/(2\Delta T \tan \beta)$$
$$= (\alpha_{11} - \alpha_{33})/(2 \tan \beta).$$

By solving the secular equation, the following expressions for the principal coefficients of thermal expansion are obtained:

$$\alpha_1 = [(1 + 1/\sin \beta)\alpha_{11} + (1 - 1/\sin \beta)\alpha_{33}]/2;$$
$$\alpha_3 = [(1 - 1/\sin \beta)\alpha_{11} + (1 + 1/\sin \beta)\alpha_{33}]/2;$$

and the Φ angle is given by

$$\Phi = \tan^{-1}[(\alpha_3 - \alpha_{33})/\alpha_{13}] = (\beta - 90°)/2.$$

The two features of the thermal-expansion ellipsoid, i.e., its strong anisotropy $[2(\alpha_3 - \alpha_1)/(\alpha_3 + \alpha_1) = 0.57]$ and its symmetrical orientation with respect to the lattice, will be related below to structural changes with temperature.

Room-temperature structure

Bond distances in the coordination polyhedra are reported in Table 4. All structural features of piemontite after Dollase (1969) are substantially confirmed, includ-

Table 3. Lattice thermal-expansion coefficients

	a	*b*	*c*	*V*
p_0	8.883(2) Å	5.682(1) Å	10.199(1) Å	465.6(1) Å³
k	6.6(3) × 10⁻⁵ Å/°C	5.6(2) × 10⁻⁵ Å/°C	12.8(2) × 10⁻⁵ Å/°C	0.0140(1) Å³/°C
r	0.99	1.00	1.00	1.00
α	0.75(4) × 10⁻⁵ K⁻¹	0.98(5) × 10⁻⁵ K⁻¹	1.26(5) × 10⁻⁵ K⁻¹	3.01(6) × 10⁻⁵ K⁻¹

Note: Estimated standard deviation are in parentheses. Coefficients from linear-regression analysis of temperature dependence of lattice parameters, $p = kT + p_0$, correlation coefficient (r), and coefficients of thermal expansion (α) between 25 and 800 °C for piemontite.

Table 4. Lengths (Å) of cation–oxygen bonds in piemontite, polyhedra volumes (Å^3), and coefficients of thermal expansion α (10^{-6} K^{-1})

	25 °C	800 °C	α
Si(1)–O(1) ×2	1.653(1)	1.642(3)	−9
–O(7)	1.569(2)	1.558(4)	−9
–O(9)	1.639(2)	1.638(4)	−1
Average	1.629	1.620	−7
Volume	2.207(4)	2.173(7)	−20
Si(2)–O(3) ×2	1.622(1)	1.616(3)	−5
–O(8)	1.603(2)	1.607(4)	3
–O(9)	1.635(2)	1.630(4)	−4
Average	1.621	1.617	−3
Volume	2.181(4)	2.170(7)	−7
Si(3)–O(2) ×2	1.627(1)	1.625(3)	−2
–O(5)	1.667(2)	1.672(4)	4
–O(6)	1.644(2)	1.652(4)	6
Average	1.641	1.644	2
Volume	2.254(4)	2.263(7)	5
A(1)–O(1) ×2	2.460(1)	2.490(3)	16
–O(3) ×2	2.333(1)	2.372(3)	21
–O(5)	2.545(2)	2.562(4)	9
–O(6)	2.849(2)	2.841(4)	−4
–O(7)	2.294(2)	2.313(4)	12
–O(9) ×2	3.043(1)	3.051(1)	3
Average	2.596	2.616	10
Volume	27.38(1)	28.32(2)	44
A(2)–O(2) ×2	2.732(1)	2.735(3)	1
–O(2)′ ×2	2.556(1)	2.608(3)	26
–O(3) ×2	2.718(1)	2.727(3)	4
–O(7)	2.285(2)	2.323(4)	21
–O(8) ×2	3.028(1)	3.050(1)	9
–O(10)	2.569(2)	2.627(4)	29
Average	2.692	2.719	13
Volume	43.44(2)	44.93(4)	44
M(1)–O(1) ×2	1.947(1)	1.960(3)	9
–O(4) ×2	1.868(1)	1.873(3)	4
–O(5) ×2	1.980(1)	1.999(3)	12
Average	1.932	1.944	8
Volume	9.531(7)	9.71(1)	24
M(2)–O(3) ×2	1.857(1)	1.868(3)	8
–O(6) ×2	1.938(1)	1.960(3)	15
–O(10) ×2	1.876(1)	1.879(3)	2
Average	1.890	1.902	8
Volume	8.932(7)	9.10(1)	24
M(3)–O(1) ×2	2.264(1)	2.308(3)	25
–O(2) ×2	2.026(1)	2.054(3)	18
–O(4)	1.906(2)	1.897(4)	−6
–O(8)	1.863(2)	1.863(4)	0
Average	2.058	2.081	14
Volume	11.167(8)	11.53(1)	41

Note: Estimated standard deviations are in parentheses.

ing the attachment of H to O(10) with O(4) as acceptor of the hydrogen bond [O(10)–H = 0.75(7) Å, O(4)···H = 2.24(6) Å, ∠O(10)–H···O(4) = 162(6)°]. The O–H distance is quite short, but that is usual with X-ray data because the electron of H is attracted by O. A possible (partial) attachment of the H atom to O(4), which is not bonded to Si, is excluded by a bond-valence calculation (Brown and Wu, 1976) [1.29 and 1.82 v.u. for O(10) and O(4), respectively, without the contribution of the H atom]. The crystal-chemical formula consistent with refined values of cation-occupation factors is $Ca(Ca_{0.80}Sr_{0.20})(Al_{0.81}M_{0.19})Al(Al_{0.06}M_{0.94})$ [(SiO_4) (Si_2O_7) O (OH)], where, in this case, M means a Mn^{3+}/Fe^{3+} mixture of average

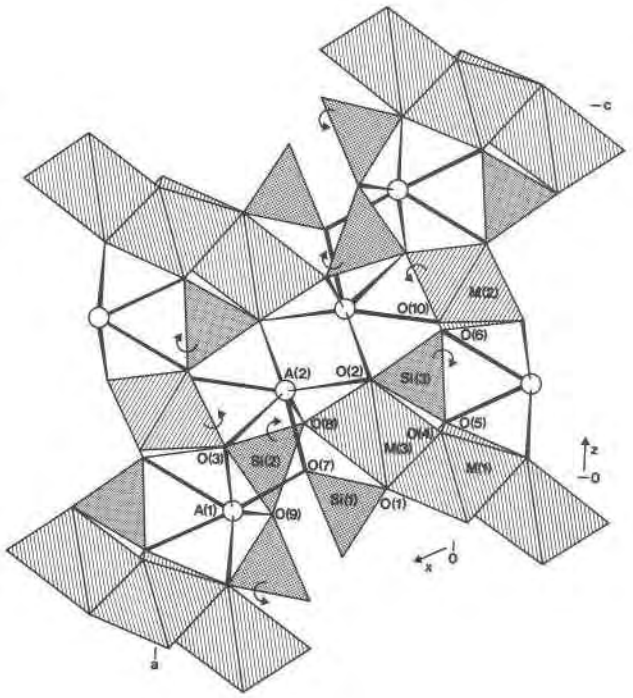

Fig. 3. Projection of the piemontite structure onto (010). Superposition hides some Ca–O bonds. Arrows show the directions of tilting of polyhedra at high temperature.

proportion about 5/2, according to microprobe analysis. All Sr goes into the A(2) site, as in Dollase's (1969) structure; in our case the Sr content is larger, but the expansion of the A(2) coordination polyhedron is slight and close to the esd's [average A–O distance of 2.692 vs. 2.688 Å for A(2) to be compared with 2.596 vs. 2.597 Å for A(1)]. We have also included the oxygen atoms at 3.043 and 3.028 Å in the coordination spheres of A(1) and A(2) because their bond-valence contributions according to Brown and Wu's (1976) formula is still appreciable (0.08 v.u.). The next-nearest oxygen atoms have the following distances: A(1)–O(9)′ × 2 = 3.37 Å, A(2)–O(8)′ × 2 = 3.39 Å.

The distribution of cations over the octahedral sites is also confirmed: the M(2) site is occupied by only Al, whereas 83% of (Mn,Fe) (80% in the previous work) goes into M(3) and the remainder into M(1). Average values of M–O bond lengths in each octahedron agree with the cation distribution from occupancy refinements. It should be emphasized that, although the M(3) octahedron is significantly larger than M(1), a small fraction of Al enters M(3) instead of M(1). This cation distribution is probably related to sharing of edges between the two kinds of octahedra, i.e., the corresponding cation sites are close enough to establish a thermodynamic equilibrium of ion migration between sites. The observed distortion of the M(3) octahedron is consistent with the well-known Jahn-Teller effect of the Mn^{3+} ion, which is the most abundant cation on this site.

A projection of the crystal structure of piemontite onto the (010) plane is shown in Figure 3. Coordination oc-

TABLE 5. RMS deviations of cation–oxygen bond distances (1), and bond angles (2), and distortion indexes (3)

	1	2	3
Si(1)	0.035	2.8	0.018
	0.036	2.8	0.019
Si(2)	0.011	1.3	0.005
	0.008	1.4	0.004
Si(3)	0.016	4.0	0.009
	0.020	4.0	0.011
M(1)	0.047	3.9	0.022
	0.053	4.1	0.024
M(2)	0.034	4.0	0.017
	0.041	4.0	0.020
M(3)	0.157	8.7	0.067
	0.176	8.6	0.073
A(1)	0.286	—	0.098
	0.274	—	0.093
A(2)	0.224	—	0.060
	0.213	—	0.052

Note: (1) $[\Sigma_i(d_i - \bar{d})^2/N]^{1/2}$ (in Å), (2) $[\Sigma_i(\Phi_i - \bar{\Phi})^2/N]^{1/2}$ (in °), and (3) $\Sigma_i|d_i - \bar{d}|/N\bar{d}$ for the cation-coordination polyhedra at 25 °C (upper values) and 800 °C (lower values) in piemontite (N = number of bonds or angles).

tahedra sharing edges form simple M(2) chains and complex M(1) and M(3) chains along [010]. These are bridged by A(1) and A(2) cations and by SiO_4 and Si_2O_7 groups.

High-temperature structure

Cation–oxygen bond lengths and polyhedra volumes of the piemontite structure at 800 °C are reported in Table 4, together with individual and average linear coefficients of bond thermal expansion in the range 25–800 °C for each coordination polyhedron. The most interesting behavior is displayed by the Si_2O_7 disilicate group, formed by the Si(1) and the Si(2) tetrahedra sharing the O(9) corner; both SiO_4 groups contract with increasing temperature instead of keeping a constant volume or expanding slightly, as usual. Hazen and Finger (1982) in their survey of high-temperature crystal-structure studies actually have given a small number of cases of negative thermal expansion coefficients for the SiO_4 tetrahedron; they have pointed out that this effect is often due to a change of structural topology, as for SiO_4 of the B chain of pyroxenes. In the pyroxene structure, the bridging O(3) atom is no longer coordinated by M(2) at high temperature; consequently, it approaches Si(B), causing a large contraction of the corresponding tetrahedron. Excluding these few "anomalous" cases, the largest negative coefficient given by Hazen and Finger (1982) is that of β-eucryptite (-8×10^{-6} K^{-1}), only slightly larger than that of Si(1) tetrahedron in the present structure (-7×10^{-6} K^{-1}).

The case of piemontite should be considered to be normal, as the coordination numbers of cations do not change at high temperature; however, the shrinking of the Si_2O_7 ditetrahedron is strong and anisotropic, so that a sharp distinction between the two cases indicated by Hazen and Finger (1982) may not be always possible. It seems that, owing to their high energy, Si–O bonds are quite insensitive to pure thermal effects, and the whole lattice expansion in silicates is accomplished by lengthening of weaker bonds, under a number of structural constraints. On the other hand, if an unbalance of bond strength received by some oxygen atoms arises, then Si–O distances may change significantly to compensate for it. This is the case for Si(1)–O(1) and Si(1)–O(7) bonds in piemontite, for instance; their substantial shortening at high temperature is clearly related to the decrease of bond strength received by O(1) and O(7), which have greatly expanded their distances to A(1) and M(3), and to A(1) and A(2), respectively (Table 4). Thus, Si–O bond lengths would act as a buffer for bond-strength unbalances, rather than responding directly to temperature changes [cf. Si(2)–O(3) as well].

The bridging angle Si(1)–O(9)–Si(2) of the Si_2O_7 group increases from 152.6° (25 °C) to 155.4° (800 °C). Even if the distortion indexes (Table 5) are practically constant, taking into account that the larger Si(1) tetrahedron contracts more than that of the smaller Si(2) (Table 4), the overall configuration of the disilicate group becomes more regular at high temperature; this increasing regularity with increased temperature occurs also to silicate chains of pyroxenes (Smyth, 1973, 1974). A quite normal thermal behavior is shown by the Si(3) isolated tetrahedron, the dimensions of which hardly change with temperature.

Considering the M(1), M(2), and M(3) coordination octahedra, the first two are characterized by thermal-expansion coefficients slightly lower than the average value for Al^{3+}–O and Fe^{3+}–O bonds given by Hazen and Finger (1982), i.e., 9×10^{-6} K^{-1}. For the Mn^{3+}–O bond, there seem to be no thermal-expansion data in the literature; however, a significantly different behavior from that of Al^{3+}–O and Fe^{3+}–O should not be reasonably expected. Thus, the observed thermal-expansion coefficient for the average M(3)–O bond length appears to be quite large, considering the M(3) site composition. The expansion of the M(3) octahedron is very anisotropic; in fact, while the two shortest bonds shrink or do not change, the two longest ones expand with some of the largest coefficients in the structure. This unusual behavior seems to be related to the Jahn-Teller effect of Mn^{3+} ions, as the corresponding distortion in the M(3) octahedron is enhanced by temperature. It should also be noted that the flattening direction of the octahedron, along O(4)–M(3)–O(8), is close to the direction of least thermal expansion of the lattice (Figs. 2, 3).

As for the A(1) and A(2) coordination polyhedra, it turns out that their average thermal expansion is rather low, particularly for A(1), with respect to the average coefficient of Ca–O bonds (Hazen and Finger, 1982) of 16×10^{-6} K^{-1}. A large anisotropy of expansion is also observed, especially in the A(2) polyhedron. This is not unexpected, however, because of the purely electrostatic nature of Ca–O coordination bonds, which makes the equilibrium bond length poorly defined. So the two bonds wiht largest thermal-expansion coefficients in the structure belong to the A(2) polyhedron: A(2)–O(10) and A(2)–O(2)′, with values of 29 and 26×10^{-6} K^{-1}, respectively; on the other hand, the longest bonds of the polyhedron

expand very little. It should be noticed that O(10) is the oxygen atom of the OH group, so that the very large lengthening of its bond to Ca at high temperature clearly signals the approaching dehydration.

In Table 5 the root-mean-square deviations from the average of bond lengths and angles together with the distortion indexes are reported for the room- and high-temperature structures; they show how the regularity of coordination polyhedra is affected by thermal expansion. Different behaviors are observed according to the types of cations: Si tetrahedra do not seem to change their distortion degree appreciably with temperature, whereas Ca-Sr polyhedra become more regular and Al-Fe-Mn octahedra less regular at high temperature. These results concern essentially the bond-length distortion, whereas bond-angle distortions are nearly insensitive to thermal effects. The behavior of coordination octahedra is in agreement with that observed in magnesiochloritoid (Ivaldi et al., 1988); a particularly large increase of distortion with thermal expansion is shown by the M(3) octahedron, in accord with the above remarks about an apparently larger Jahn-Teller effect of Mn^{3+} at high temperature. At present we are not able to propose an explanation for this result. On the other hand, by attaining a more regular configuration at high temperature, the Ca-Sr polyhedra behave consistently with the well-known tendency of crystal structures toward higher symmetry at higher temperatures.

Most bond angles within the coordination polyhedra change by less than 1° in the range 25–800 °C; the largest changes (about 1.5°) are in angles of the A(1) polyhedron involving the O(7) and O(9) atoms, which are not coordinated to octahedral cations M: O(7)–A(1)–O(1), O(7)–A(1)–O(5), O(7)–A(1)–O(6) and O(9)–A(1)–O(9)′.

The hydrogen bridge O(10)···O(4) lengthens from 2.965 to 3.023 Å, with a coefficient of thermal expansion of 25 $\times 10^{-6}$ K^{-1}, comparable with values observed for other bonds. These facts would show that the weak hydrogen bond of the OH group is still preserved at high temperature, excluding processes of deprotonation connected with oxidation reactions of octahedral cations, which are already in high valence states.

The structure-type of the epidote mineral family is close-packed along [010] but not on the (010) plane, where several coordination polyhedra are linked by simple corner-sharing. Thus, on heating we would expect not only an expansion, but also a possible rotation or tilting of polyhedra about the y crystallographic axis, as they are constrained by the (010) mirror symmetry. By comparing the orientations of octahedral chains and SiO_4 tetrahedra at room and high temperature, the following results are observed (Fig. 3). The complex M(1) and M(3) chains do not rotate, whereas the M(2) ones are tilted by about 1° (counterclockwise). The Si(1) and Si(2) tetrahedra rotate clockwise and counterclockwise, respectively, also by about 1°. The Si(3) tetrahedron undergoes a smaller clockwise tilting. The angular values given are approximate because polyhedra do not expand or contract in an exactly homogeneous way during the thermal cycle, so that the calculated orientation change depends slightly on the polyhedron edge or bond chosen for reference. Rotations of linked polyhedra sharing corners are correlated consistently; the overall effect (Fig. 3) is to allow a much larger thermal expansion along approximately the z axis than in other directions on the (010) plane. This explains the orientation of the ellipsoid of thermal expansion with respect to the lattice (Fig. 2) on a structural basis. On the other hand, the value of the largest principal coefficient (1.29 $\times 10^{-5}$ K^{-1}) is larger, on the average, than expansion coefficients of coordination polyhedra (Table 4). This expansion along z cannot be accounted for in terms of coordination bonds only, but must include effects of polyhedra tilting as well.

The breakdown of the structure

A continuous X-ray powder pattern recorded from 20 to 1140 °C (20 °C/h, Cu$K\alpha$ radiation) with a Guinier-Lenné high-temperature camera shows that the crystal structure of piemontite is basically unchanged up to about 880 °C, where it breaks down according to the following reaction: $2Ca_2Al_2(Mn,Fe)Si_3O_{12}OH \rightarrow 2CaAl_2Si_2O_8$ (anorthite) + $(Mn,Fe)_2O_3$ + 2CaO + $2SiO_2$ + H_2O; the silica should be amorphous. At about 980 °C the bixbyite-type phase decomposes and gives ramsdellite plus a manganese-iron oxide according to $6(Mn,Fe)_2O_3 + O_2 \rightarrow 2MnO_2 + 2(Mn,Fe)_5O_8$. Presumably the dehydration temperature for a single crystal could be higher than that found for a powder sample [cf. magnesiochloritoid (Ivaldi et al., 1988)].

Acknowledgments

We are indebted to P. Brizio who kindly supplied the sample of piemontite. This research has been supported by M.P.I. and C.N.R. (Advanced Crystallographic Methods) grants.

References cited

Argoud, R., and Capponi, J.J. (1984) Soufflette à haute température pour l'étude de monocristaux aux rayons X et aux neutrons jusqu'à 1400 K. Journal of Applied Crystallography, 17, 420–425.

Brown, I.D., and Wu, K.K. (1976) Empirical parameters for calculating cation-oxygen bond valences. Acta Crystallographica, B32, 1957–1959.

Deer, W.A., Howie, R.A., and Zussman, J. (1986) Rock-forming minerals: Vol. 1B, Disilicates and ring silicates. Longman, London.

Dollase, W.A. (1969) Crystal structure and cation ordering of piemontite. American Mineralogist, 54, 710–717.

Finger, L.W., and Prince, E. (1975) A system of Fortran IV computer programs for crystal structure computations. U.S. National Bureau of Standards Technical Note 854.

Hazen, R.M., and Finger, L.W. (1982) Comparative crystal chemistry. Wiley, Chichester.

Ivaldi, G., Catti, M., and Ferraris, G. (1988) Crystal structure at 25 and 700 °C of magnesiochloritoid from a high-pressure assemblage (Monte Rosa). American Mineralogist, 73, 358–364.

Mottana, A., and Griffin, W.L. (1982) The crystallochemistry of piemontite from the type-locality (St. Marcel, Val D'Aosta, Italy). Reports of 13th International Mineralogical Association Meeting, Varna, p. 635–640.

North, A.E.T., Phillips, D.C., and Mathews, F.S. (1968) A semiempirical method of absorption correction. Acta Crystallographica, A24, 351–359.

Schlenker, J.L., Gibbs, G.V., and Boisen, M.B., Jr. (1978) Strain-tensor components expressed in terms of lattice parameters. Acta Crystallographica, A34, 52–54.

Smyth, J.R. (1973) An orthopyroxene structure up to 800 °C. American Mineralogist, 58, 636–648.

——— (1974) The high temperature crystal chemistry of clinohyperstene. American Mineralogist, 59, 1069–1087.

Manuscript received February 25, 1988
Manuscript accepted June 28, 1988